Article:
Papargyriou, I. and Hajirasouliha, I. (2022) Performance-based seismic design and assessment of multi-storey CFS strap-braced frames. Engineering Structures, 261. 114268. ISSN: 0141-0296

https://doi.org/10.1016/j.engstruct.2022.114268

Performance-Based Seismic Design and Assessment of Multi-Storey CFS Strap-Braced Frames

Ioannis Papargyriou[a*], Iman Hajirasouliha[a]

[a] Department of Civil and Structural Engineering, The University of Sheffield, S1 3JD, Sheffield, UK

* Corresponding author; E-mail: i.papargyriou@sheffield.ac.uk

Abstract

Cold-formed steel (CFS) structures typically rely on diagonally braced stud walls to withstand lateral forces. While the response of CFS single-wall panels has been extensively investigated, limited studies focused on the seismic performance of multi-storey CFS strap-braced frames. Previous research highlighted that the presence of vertical loading can significantly reduce the lateral load and ductility capacity of strap-braced walls by amplifying the secondary moments due to P-Δ effects. While this effect is generally ignored in current design practice, it may lead to premature failures and poor seismic performance. This study aims to investigate the efficiency of a new design methodology to take into account the vertical load effects on the performance of multi-storey CFS strap-braced frames. Detailed experimentally validated FE models of CFS panels were developed in ABAQUS and used to obtain equivalent hysteretic models in OpenSees. The seismic performance of 6-storey strap-braced frames designed based on the Eurocode 8 and the proposed design methodology were then investigated under a set of artificial spectrum-compatible records. While the code-base design did not satisfy the ASCE/SEI 41-17 Life Safety (LS) and Collapse Prevention (CP) ductility limits, all performance targets were met using the proposed design methodology. The results of Incremental Dynamic Analyses (IDA) also indicated that meeting the code capacity requirements could not prevent extensive global damage in the strap-braced frames, due to soft-storey failure modes associated with the premature buckling of chord studs. Finally, the

efficiency of the proposed design compared to its code-compliant counterpart was demonstrated under a set of 20 real spectrum compatible records, showing higher ductility capacity and considerably lower damage levels.

Keywords: Cold-formed Steel (CFS); Strap-Braced Frames; Ductility; Performance-Based Design; Incremental Dynamic Analysis (IDA); Global Damage Index.

1 Introduction

Cold-Formed Steel (CFS) structural systems are increasingly used in modern construction practices due to their unique advantages, such as lightweight, flexibility in cross-sectional shapes, and ease of handling and transportation compared to conventional hot-rolled steel structures. In conventional multi-storey CFS buildings, strap-braced stud walls are widely used as one of the primary force-resisting system against lateral wind and earthquake loads. The lateral resistance is generally provided by diagonal X-shaped bracing members [1], while knee-braced [2], K-braced [3–5], or a combination of K- and X-shaped braces [6] have also been utilised. Previous studies indicated that the structural response of the strap-braced stud walls can be considerably affected by the wall's aspect ratio [7–9]. It was shown that ratios greater than 1:2 might lead to a less ductile behaviour due to the premature failure of the chord studs. Studies on the performance of walls employing welded joints [8,9] suggested a ductile response, provided a careful design and fabrication are implemented. In common practice, CFS strap-braced walls are sheathed with a wide range of materials like gypsum, OSB or plywood boards. Although they can increase the lateral load capacity through their stiffness [10], a composite action with the diagonal braces is not accounted for in the current design codes as a result of their brittle nature [11].

Under seismic load actions, diagonally strap braced systems dissipate energy mainly by the plastic deformation of the tensile straps, as the straps in compression buckle at a very early loading stage due to their high width-to-thickness ratio (or high slenderness). Although the straps usually have a uniform cross-section over their total length, it has proven beneficial to reduce the width over a length in the middle, acting as a seismic fuse and protecting the susceptible elements such as the connections of the straps with the chord studs [1]. Currently, the primary approach to avoid brittle modes of failure in CFS stud wall systems is achieved by implementing capacity design rules. The aim is to provide non-dissipative members with a desirable level of over-strength, to sustain the maximum forces anticipated in the plastic regions. This eventually allows the system to develop ductility (i.e. the ability to experience large plastic deformations while maintaining their yield capacity) through yielding at controlled locations [12,13]. The highest ductility capacity can be attained if the braces have sufficient ductility [14–16] and premature failure modes in the chord studs are prevented before the diagonal straps reach their ultimate strain [17].

There are limited experimental research studies on the seismic response of CFS multi-storey systems employing diagonal braces. Aiming to study the non-linear dynamic behaviour of CFS structural systems, Kim et al. [18] performed full-scale shaking table tests on two-storey one-bay strap-braced frames with box-shaped chord studs and welded connections. A maximum drift ratio of 3% at the first storey was reported, and no obvious damage was observed, confirming the suitability of the system for seismic applications. In a similar study, Fiorino et al. [19] tested three-storey two-bay CFS strap-braced wall frames designed per Eurocode 8 as non-dissipative systems. The system exhibited satisfactory performance and achieved a maximum drift ratio of over 2%, without significant damage.

In their numerical study at the structural level, Lee and Foutch [20] performed a modified incremental dynamic analysis of two-, four- and six-storey strap-braced wall frames,

employing twenty accelerograms. They concluded that the R factor of 4 was adequate for this system, while the per FEMA 355F [21] estimated collapse drift capacities were too conservative. Velchev [1] and Comeau et al. [22] assessed the AISI S213 Canadian and FEMA P695 seismic force modification factors, alongside the building height limits for multi-storey concentrically strap-braced systems. Their studies, in general, confirmed the code suggested values for limited ductility (LD) and conventional construction (CC) systems. In another relevant study, Fiorino et al. [23] conducted a numerical study following FEMA P695 [24] specifications to assess the behaviour factor for CFS strap-braced stud wall systems. They investigated the seismic performance of a set of fourteen archetypes using CFS strap-braced stud walls featuring screwed connections with gusset plates. The results indicated the suitability of the system for seismic applications; however, the studied structures exhibited a relatively low behaviour factor (q) around 2.5. Davani et al. [25] also evaluated the performance of nine full-scale wall specimens based on the experimental work of Moghimi and Ronagh [11], subjected to 14 ground motions. Their study showed that the contribution of cladding and corner brackets can increase the lateral strength and stiffness and reduce the occurrence of damage in strap-braced wall systems.

Experimental test studies on the monotonic and cyclic response of single-wall panels were generally conducted without accounting for any additional vertical loads. Additional vertical loads have been applied only in a few experimental studies focusing on sheathed walls without employing diagonal straps [26–28]. However, due to their inherently different mechanism, the results do not apply to strap-braced systems. It should be noted that Eurocode 8 [29] does not contain explicit design rules for CFS stud wall systems, and the ones intended for conventional hot-rolled steel structures are generally used. Following these, the lateral load capacity of strap-braced walls is based on the tensile strength of the straps alone, under zero vertical loading. Therefore, the secondary bending moments due to P-Δ effects are not currently accounted for

in the seismic design of CFS strap-braced stud wall systems. AISI S400-20 [30] accounts for the bending moment due to P-Δ effects, but for walls with a height-to-width ratio greater than 1.9:1. However, research recently conducted by Papargyriou et al. [17] suggested that the lateral load and ductility capacities of strap-braced wall systems were adversely affected by additional vertical loads leading to premature failure modes in the chord studs due to P-Δ effects, even for 1:1 ratios.

In a recent study by Papargyriou and Hajirasouliha [31], a new methodology was developed for designing CFS strap-braced wall frames, proposing preliminary design formulae to predict the lateral load and ductility capacity of strap-braced stud walls, considering different cross-sectional thicknesses and vertical load levels. The efficiency of the proposed method was demonstrated by designing a CFS 6-storey frame following Eurocodes' guidelines. It was shown that although the member capacity checks were satisfied, the ductility of the system was well below the target ductility at some storey levels, yielding a brittle response and an unacceptable seismic performance. By applying their proposed methodology, however, the design solution could satisfy both the Eurocode capacity checks and the target ductility demands at different earthquake intensity levels.

The present work aims to assess the efficiency of the design methodology proposed by Papargyriou and Hajirasouliha [31], for the first time, at the structural level and provide a better understanding of the seismic performance of CFS strap-braced multi-storey systems by quantifying their global damage and failure mechanism at different earthquake intensity levels. Detailed non-linear FE models of CFS panels are developed in ABAQUS [32], and their accuracy is demonstrated against experimental results in the literature. To increase the computational efficiency, the validated models are then used to obtain equivalent hysteretic models in OpenSees [33]. The seismic performance of 6-storey strap-braced frames designed based on the Eurocode-8 and the proposed design methodology is then investigated under a set

of artificial spectrum-compatible records under increasing intensity (i.e. incremental dynamic analyses) as well as twenty real earthquake ground motion records representing the selected design spectrum. Finally, the efficiency and reliability of the design solutions are assessed based on ASCE/SEI 41-17 ductility limits for different performance levels, wall ductility capacities obtained from the validated FE models in ABAQUS, and a global cumulative damage index. The results indicated that the Eurocode design solution, ignoring the effect of vertical loads in the ductility capacity, did not fulfil the Life Safety (LS) and Collapse Prevention (CP) performance levels and sustained extensive damage even at low earthquake intensity levels. However, the proposed methodology yielded improved seismic performance with higher ductility capacity and significantly lower damage levels.

2 Proposed design methodology

In a previous study by Papargyriou et al. [17], it was found that additional vertical loads imposed to a CFS strap-braced stud wall led to increased secondary moments in the compressive chord stud due to P-Δ effects. The interaction of the axial loads and the secondary moments can result in the premature buckling failure of chord studs before straps reach their ultimate strain and subsequently reduce the lateral load-bearing capacity and ductility of the system. To address this issue, Papargyriou and Hajirasouliha [31] proposed a design methodology to estimate the lateral load-bearing and ductility capacity of CFS strap-braced stud walls under the presence of vertical loads. Their proposed procedure can be summarised as follows:

- Step 1: The lateral response of a reference CFS strap-braced stud wall (wall 1) under monotonic loading is obtained using a detailed FE model or experimental test results. No vertical load is applied at this stage, and therefore the failure mode is expected to be due to gross cross-section rupture of the straps.

- Step 2: Under zero vertical loading, Eq. (1) is used to calculate the lateral load capacity ($F_{u,2}$) of a selected CFS strap-braced stud wall (wall 2) with the same configuration and material properties as wall 1, but different element sizes. It is related to the lateral load capacity of wall 1 ($F_{u,1}$), calculated in the previous step, as a function of the diagonal strap thicknesses ($t_{s,1}$) and ($t_{s,2}$) and chord stud thicknesses ($t_{ch,1}$) and ($t_{ch,2}$) of walls 1 and 2, respectively.

$$F_{u,2} = F_{u,1} \cdot f1\left({}^{t_{s,2}}/_{t_{s,1}}, {}^{t_{ch,2}}/_{t_{ch,1}}\right) \quad (1)$$

- Step 3: The ductility of reference wall 1 (μ_1), calculated in step 1, is used to estimate the ductility of wall 2 (μ_2) under the condition of zero vertical loading, with the aid of Eq. (2).

$$\mu_2 = \mu_1 \cdot f2\left({}^{t_{s,2}}/_{t_{so,2}}\right) \quad (2)$$

In the above equation ($t_{so,2}$) is the diagonal strap thickness of wall 2, which leads to the simultaneous failure of the strap and the chord stud. A simple design process is proposed to obtain ($t_{so,2}$) using the axial-bending moment interaction relationship $F_c/N_{cRd}+M/M_{c,Rd}=1$, where (F_c) is the compressive component of the strap force transferred on the chord stud, ($N_{c,Rd}$) and ($M_{c,Rd}$) are the compressive and bending moment capacities of the chord stud, respectively, calculated in accordance with EN 1993 [34,35], and (M) is the secondary bending moment due to P-Δ effects.

- Step 4: At this stage, Eqs. (3) and (4) are used to predict the lateral load capacity ($F_{u,P,2}$) and ductility ($\mu_{P,2}$) of wall 2, under the presence of a vertical load (P), expressed as a ratio against the total vertical load capacity of the wall ($P_{w,2}$), obtained by adding the axial load capacities of the intermediate and chord studs calculated per Eurocode 3 [34,35].

$$F_{u,P,2} = F_{u,2} \cdot f3\left({}^{P}/_{P_{w,2}}\right) \quad (3)$$

$$\mu_{P,2} = \mu_2 \cdot f4\left({}^{P}/_{P_{w,2}}\right) \quad (4)$$

The functions f1, f2, f3 and f4 were obtained based on the results of a comprehensive parametric study conducted by Papargyriou and Hajirasouliha [31] on a wide range of CFS strap-braced stud walls. Table 1 lists the adopted functions for the wall configuration used in this study (see Fig. 1). It should be noted that while the proposed design methodology is general, these functions may slightly change if a very different bracing system is utilised.

Table 1 Functions f1, f2, f3 and f4 used to obtain lateral load capacity and ductility per Eqs. (1), (2), (3) and (4) (adopted from Papargyriou and Hajirasouliha [31])

$f1 = \frac{F_{u,2}}{F_{u,1}} = 0.85\left(\frac{t_{s,2}}{t_{s,1}}\right) + 0.15\left(\frac{t_{ch,2}}{t_{ch,1}}\right)$
$\begin{cases} f2 = \frac{\mu_2}{\mu_1} = 1, & t_{s,2} \le t_{so,2} \\ f2 = \frac{\mu_2}{\mu_1} = -0.09 + 2.16\left(\frac{t_{s,2}}{t_{so,2}}\right) - 1.07\left(\frac{t_{s,2}}{t_{so,2}}\right)^2, & t_{s,2} > t_{so,2} \end{cases}$
$f3 = \frac{F_{u,P,2}}{F_{u,2}} = 1 - 0.60\left(\frac{P}{P_{w,2}}\right) + 0.30\left(\frac{P}{P_{w,2}}\right)^2$
$f4 = \frac{\mu_{P,2}}{\mu_2} = \mathrm{A}\left(\frac{P}{P_{w,2}}\right)^3 + \mathrm{B}\left(\frac{P}{P_{w,2}}\right)^2 + \mathrm{C}\frac{P}{P_{w,2}} + 1$ $A = 10.47\left(\frac{t_{s,2}}{t_{so,2}}\right)^3 - 44.19\left(\frac{t_{s,2}}{t_{so,2}}\right)^2 + 30.69\left(\frac{t_{s,2}}{t_{so,2}}\right) + 4.85$ $B = -8.55\left(\frac{t_{s,2}}{t_{so,2}}\right)^3 + 31.65\left(\frac{t_{s,2}}{t_{so,2}}\right)^2 - 18.64\left(\frac{t_{s,2}}{t_{so,2}}\right) - 7.47$ $C = -1.75\left(\frac{t_{s,2}}{t_{so,2}}\right)^3 - 5.95\left(\frac{t_{s,2}}{t_{so,2}}\right)^2 + 3.05\left(\frac{t_{s,2}}{t_{so,2}}\right) + 0.81$

2.1 Design solutions of a case study frame

To demonstrate the efficiency of the proposed methodology, a case study multi-storey CFS frame was designed following Eurocodes' specifications. The frame had six storeys above ground level, each having a height of 2.74 m, and three 2.44 m span bays. The middle span at

each level was configured as the strap-braced wall panel, providing the lateral bearing resistance (see Fig. 1). The cross-sectional dimensions of the walls' elements, including the studs, the top and bottom tracks, the bridging element, and the diagonal straps, are shown in Fig. 1. The chord studs consisted of two back-to-back single lipped-channel sections, while the diagonal straps had a "dogbone" shape, having a reduced depth over a length of 762 mm in the middle. The thicknesses of the studs and the diagonal straps varied along the frame height. A tributary width of 5.0 m was assumed for the calculation of the gravity loads and the storey masses.

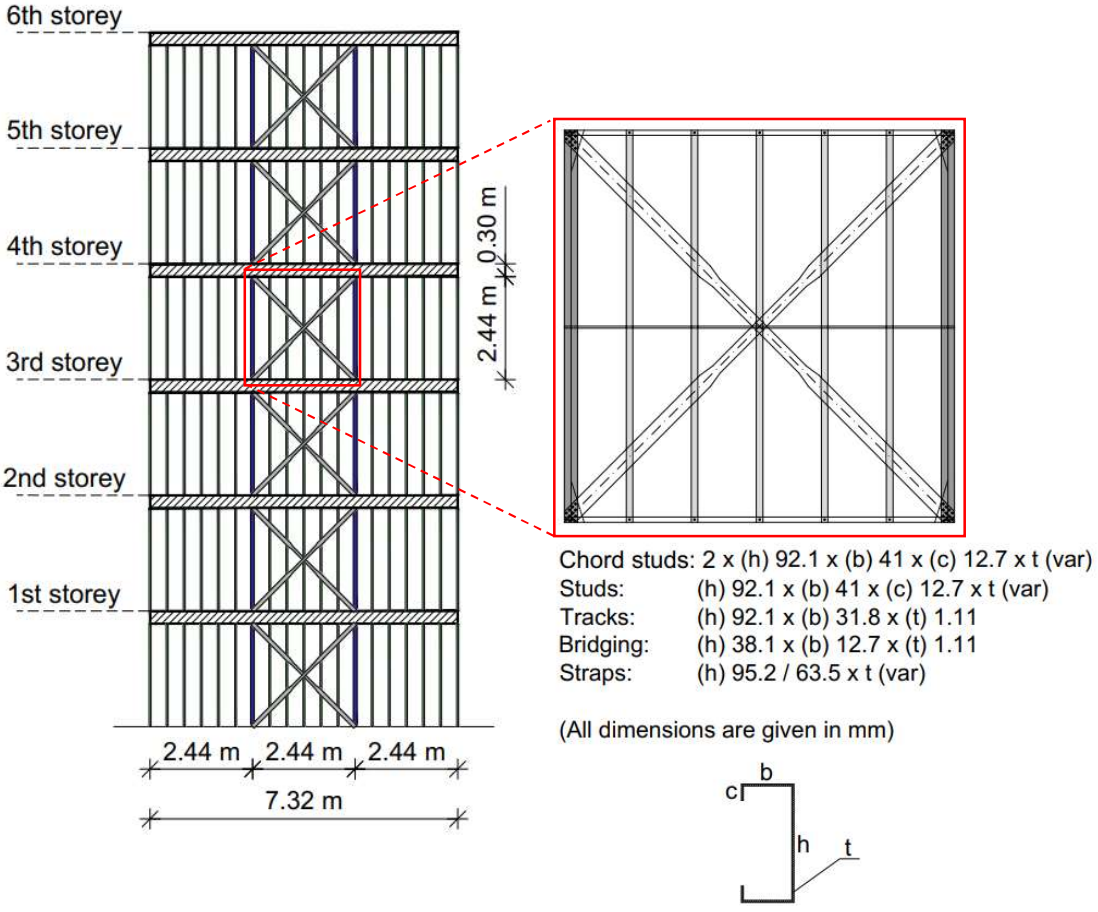

Fig. 1 Geometry of the case-study strap-braced wall frame

2.2 Design specifications

The frame was assumed to be part of a residential-use building, of importance class II, designed for a permanent load $g = 1.5$ kN/m^2 and a live load $q = 2$ kN/m^2, while the partial

196 safety factors per EN 1990 [36] were γ_G=1.35 and γ_Q=1.50, respectively. The storeys all had
197 equal masses, calculated from the combination of the seismic action in accordance with
198 EN 1990 [36]: $G_k + \psi_{E,i} \cdot Q_k$, where ($G_k$) and ($Q_k$) represent the permanent and variable (live)
199 loads, respectively, and ($\psi_{E,i}$) is the coefficient for variable actions taken as 0.3. The site was
200 assumed to be in a high seismicity area, with a reference peak ground acceleration α_{gR}=0.35 g
201 and a ground type B (i.e. deposits of very dense sand, gravel, or very stiff clay). The building
202 was assumed to be regular in plan and elevation, and the base shear force was calculated and
203 distributed along the height following the lateral force method per Eurocode 8 [29].

204 *2.3 Conventional and proposed design solutions*

205 For the conventional design solution, the frame members were designed in accordance
206 with Eurocode 3 [34,35] and the capacity design rules of Eurocode 8 [29]. However, as
207 discussed before, the effects of vertical loads on the lateral load capacity and ductility of the
208 strap-braced wall frames are not taken into account in the Eurocode design process. To address
209 and further study this issue, the same frame was designed following the proposed methodology,
210 explained in section 2 (proposed design solution). The thicknesses of the studs (t_{ch}) and the
211 diagonal straps (t_s) of the Eurocode and the proposed design solutions are listed in Table 2,
212 while the general dimensions of the sections are shown in Fig. 1.

213 Following an eigenvalue analysis, the fundamental periods of the Eurocode and the
214 proposed design solutions were 0.82 sec and 0.78 sec, respectively. It should be noted that the
215 period used for the initial design of the frames was 0.408 sec and calculated based on EC8
216 proposed design equation.

Table 2 The plate thickness of the members in the Eurocode and the proposed design solutions (sizes are shown in Fig. 1)

	Eurocode design		Proposed design	
Storey No	**Stud thickness t_{ch}** (mm)	**Diagonal strap thickness t_s** (mm)	**Stud thickness t_{ch}** (mm)	**Diagonal strap thickness t_s** (mm)
1	2.0	4.0	2.0	4.0
2	1.5	4.0	2.0	4.0
3	1.5	4.0	2.0	4.0
4	1.16	3.0	1.5	3.0
5	1.16	3.0	1.5	3.0
6	1.16	1.5	1.16	1.5

3 Development of non-linear numerical models

Numerical modelling has been widely used as a cost-effective and efficient means to predict the response of CFS elements and structural systems under different loading conditions [5,37]. In this study, ABAQUS software [32] was utilised to simulate the non-linear behaviour of CFS strap-braced wall panels, as previous studies showed that it can provide accurate results for thin-walled CFS elements and connections [38–41]. The developed models were validated against available experimental data and were then used to: a) derive the load-displacement curves for the wall panels of the Eurocode and the proposed design solutions, as discussed in section 2, and b) obtain equivalent non-linear hysteretic models in OpenSees software [33] to simulate the non-linear seismic behaviour of multi-storey CFS strap-braced frames under different earthquake intensity levels. Using this approach can significantly reduce the computational costs of non-linear dynamic analyses of such complex systems. However, it should be noted that, in general, the wall panels have a different lateral response at each storey, depending on their cross-sectional dimensions and the amount of vertical loading, and therefore equivalent models should be obtained for them individually.

3.1 *Detailed non-linear numerical model in ABAQUS*

As shown in Fig. 2, the detailed wall models in ABAQUS comprised the chord and intermediate studs, the top and bottom tracks, and the bridging element at the mid-height of the wall. Two pairs of diagonal dogbone-shaped straps were used as bracing elements. The element dimensions are shown in Fig. 2. The model accounted for material non-linearity and P-Δ effects. The initial geometric imperfections were omitted in this work since previous studies [17] showed that they had a negligible effect on the lateral response of the system. **Table 3** summarises the engineering values of yield (f_y) and ultimate (f_u) stresses for the structural elements. The modulus of elasticity (E) and the Poisson's ratio (ν) had values of 203 GPa and 0.3, respectively.

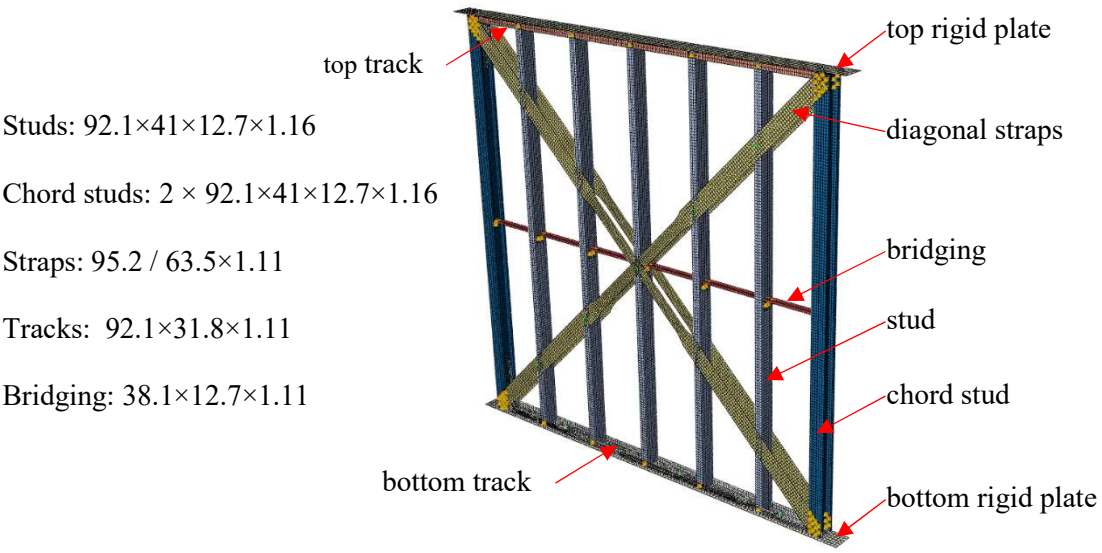

Fig. 2 Detailed ABAQUS numerical model

Table 3 Material properties of ABAQUS model

Element	**Yield stress f_y** (MPa)	**Ultimate stress f_u** (MPa)
Straps	296	366
Studs / Chord studs	325	382
Tracks	296	366

In the following section, the key features of the developed FE model are presented. For a more thorough description and discussion, the reader can refer to [17].

3.1.1 Summary of model features

Similar to the reference experimental test set-up, the developed models featured the hold-down devices and anchor rods at the chord stud top and bottom ends alongside the connections of the tracks through shear anchors. Over the top and below the bottom track, rigid plates were used to transfer the vertical loads uniformly to the chord studs, the intermediate studs and the foundation. The bridging element, intended to reduce the effective length of the vertical elements, was attached to them through L-shaped brackets.

The ABAQUS "S4R" shell element (four-node element with three translational and three rotational degrees of freedom per node) was used to discretise the wall's elements as it was proven accurate in predicting the behaviour of CFS systems in the previous studies [38,39,41]. Following a mesh sensitivity analysis, the lateral load capacity value converged at a mesh size of 15 mm × 15 mm, yielding a difference of less than 0.5% compared to a coarser mesh of 20 mm × 20 mm.

The straps were connected to the chord studs and the top and bottom tracks through 12 No 10 (∅10 mm) self-drilling screws, while the intermediate studs were connected to the top and bottom tracks through 1 No 8 (∅8 mm) self-drilling screw per side, at each end. The screwed connections were modelled using discrete fasteners, which were assigned connector properties, defining the relative motion between the connected surfaces. The proposed equations in Pham and Moen's work [42], derived based on their experimental work on steel screw-fastened connections, were adopted to describe the strength and stiffness of the connectors.

The vertical load was applied in the first analysis step as a uniformly distributed surface load on the rigid top plate, and the lateral displacements were imposed in the second step. A

maximum displacement value of 300 mm was applied for monotonic analysis, whereas cyclic loading followed the reversed cyclic protocol suggested by ASTM E2126 [43] , as shown in Fig. 3.

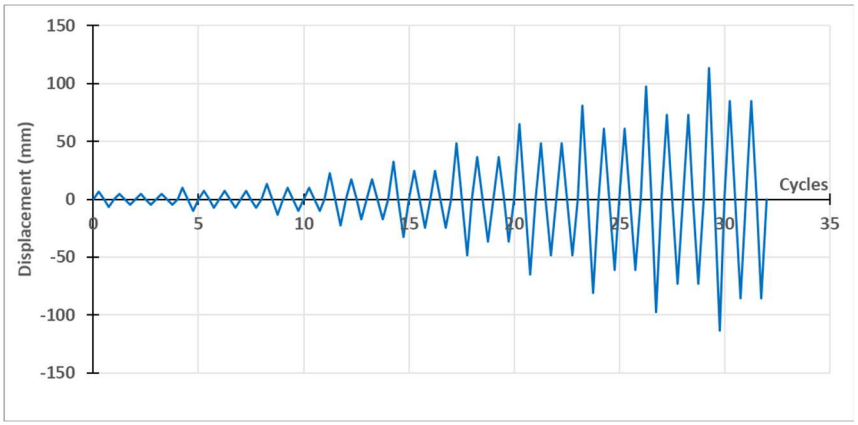

Fig. 3 Reversed cyclic protocol per ASTM E2126 [43]

In order to transfer the vertical load and account for the correct interaction between the structural elements, surface-to-surface interactions were described, using a "hard" contact definition in the normal direction and a "frictionless" contact in the transverse direction.

3.1.2 Model validation

The developed FE model was verified under cyclic loading against the results of test specimens 26A-C and 32A-C included in the experimental work of Velchev [1]. The lateral load-displacement responses of the test and the FE analyses are compared in Fig. 4. The results, in general, demonstrate the efficiency of the adopted FE models to simulate the hysteretic response of the tested CFS strap-braced walls. The average error in the estimated cumulative energy dissipation (i.e. the area enclosed by the load-displacement curves) of the walls was 18% and 17% for the test specimens 26A-C and 32A-C, respectively. A more comprehensive comparison can be found in [17].

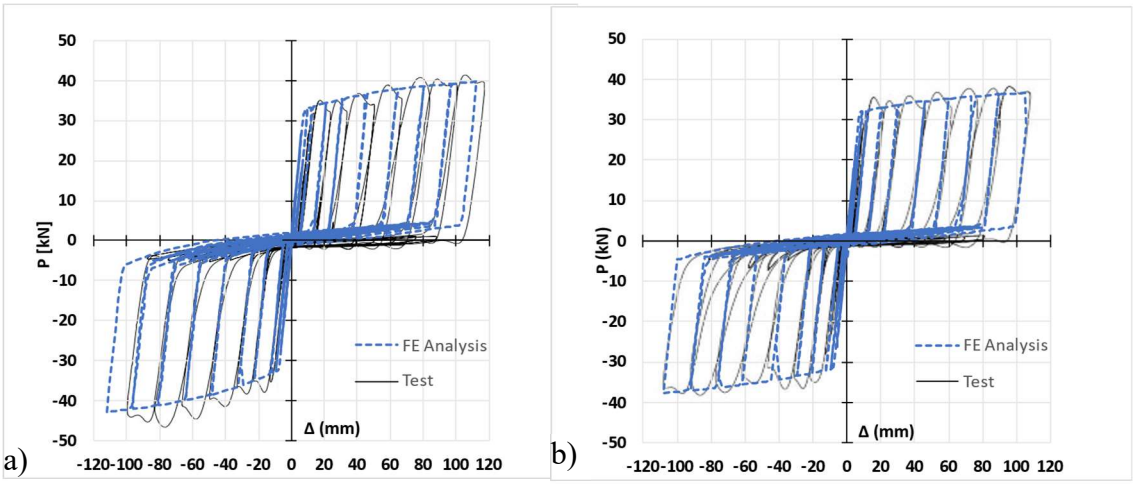

Fig. 4 Comparison of the experimental and FE analysis predicted cyclic responses of specimens a) 26A-C, and b) 32A-C

To assess the efficiency of the Eurocode and the proposed design methodology in terms of the lateral load capacity and ductility of the wall panels, the validated FE models were adopted to obtain the load-displacement curves for all the wall panels of the Eurocode and the proposed design solutions by taking into account their cross-sectional dimensions and the amount of vertical loading. The results were then used to calculate the ultimate load capacity (F_u) and ductility (μ) for each wall panel. Ductility was expressed as a ratio of the ultimate displacement (Δ_u) over the displacement at yield (Δ_y) (i.e. $\mu = \Delta_u/\Delta_y$). The ultimate displacement was taken as the minimum of the displacement corresponding to the failure of the wall (due to strap rupture or buckling of the compressive chord stud) or the displacement corresponding to a 20% drop of the ultimate load capacity. To obtain the values of (Δ_u) and (Δ_y), idealised bilinear curves of the actual responses, based on the FEMA 356 [44], were used.

The ultimate lateral load (F_u) and ductility (μ) capacities of the walls at each storey level are summarised in Table 4 for the Eurocode and the proposed design solutions. It can be noted that, despite satisfying the code's load capacity checks, the Eurocode design solution exhibits relatively low ductility capacity at storeys 2 to 5, well below the target ductility of 4 expected for ductility class medium (DCM) structures. As discussed before, this is mainly attributed to

312 the premature buckling of the chord studs caused by the interaction of the compressive force
313 and secondary moment due to P-Δ effects, amplified by the presence of vertical loads. By
314 contrast, the proposed design solution reached high ductility values at all storeys.
315
316 **Table 4** Lateral load and ductility capacities of the Eurocode and the proposed design solutions

Storey No	Eurocode design		Proposed design	
	F_u (kN)	μ	F_u (kN)	μ
1	120.4	14.8	120.3	14.8
2	105.2	1.9	121.7	15.5
3	108.8	2.1	123.1	15.9
4	80.7	2.4	93.0	15.3
5	85.5	2.6	94.4	16.3
6	49.1	21.3	49.1	21.3

317
318 *3.2 Non-linear numerical models in OpenSees*
319 In this study, OpenSees software [33] is used to assess the seismic performance of multi-
320 storey CFS strap-braced frames. Fig. 5 shows the OpenSees numerical model of a single wall
321 panel. It comprised the intermediate and chord studs, the top track and one diagonal element
322 that represents the overall hysteretic behaviour of the X-shaped braces. The studs and chord
323 studs were modelled with "truss" elements and assigned elastic "uniaxialMaterial" properties.
324 The top track was modelled using the "elasticBeamColumn" element, which supports
325 uniformly distributed loading and incorporates elastic material properties. The non-linear
326 lateral behaviour of the wall was simulated by using the diagonal element with the non-linear
327 "Pinching4" material, derived from the corresponding monotonic analysis of detailed
328 ABAQUS numerical models for each wall panel. In practical terms, this single diagonal
329 element controls the non-linear lateral performance of the wall, while the effects of local
330 buckling and failure of all the elements on the overall response of the system are indirectly
331 included. This is explained in more detail in the next section.

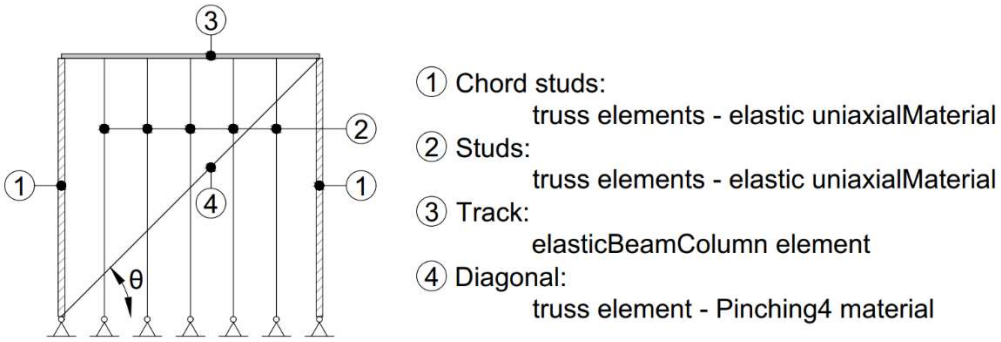

Fig. 5 Single strap-braced wall model in OpenSees

3.3 Hysteretic response

In general, strap-braced stud walls subjected to cyclic loading exhibit a pinching behaviour, which results from only the tensile straps being active in every excursion [18]. Therefore, in this study, the hysteretic response of the wall was defined by assigning the hysteretic "Pinching4" material (see Fig. 6) of OpenSees [33] to the diagonal element which in previous studies [23,45] was proven accurate in capturing this behaviour.

The "Pinching4" material definition comprises 39 parameters, including the backbone curve points of the cyclic response for both positive and negative loading directions, the pinching, and finally, the strength and stiffness degradation parameters. Since neither strength nor stiffness degradation was observed in the studied walls, their corresponding parameters were set equal to zero.

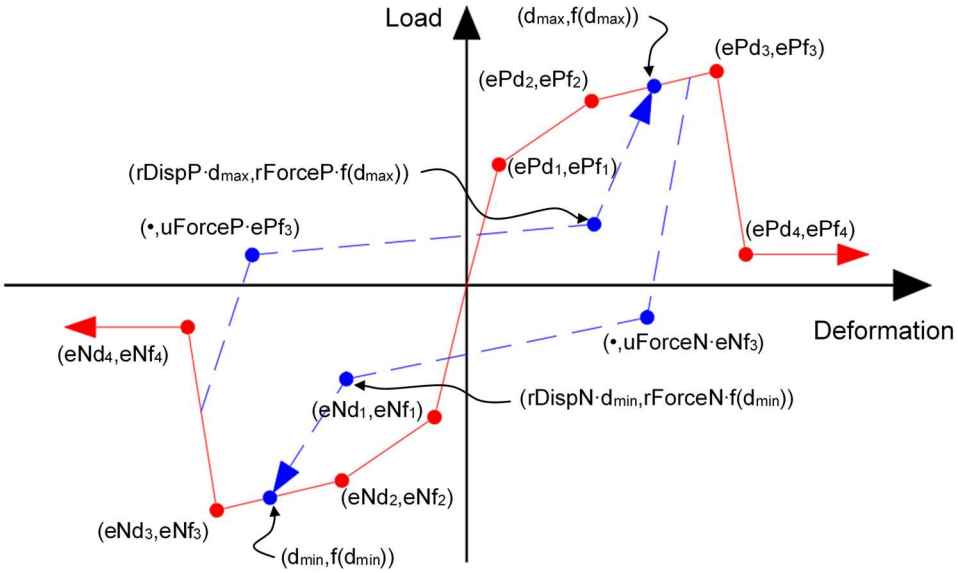

Fig. 6 Definition of OpenSees [33] "Pinching4" hysteretic model

The point pairs (ePd_1, ePf_1), (ePd_2, ePf_2), (ePd_3, ePf_3) and (ePd_4, ePf_4), defining the positive loading direction backbone envelope, were selected from the bi-linearised, per FEMA 356 [44], monotonic lateral load-displacement relationship of the corresponding ABAQUS numerical models, whilst the pairs (eNd_1, ePf_1), (eNd_2, ePf_2), (eNd_3, ePf_3) and (eNd_4, eNf_4), representing the negative-loading backbone curve were set equal to their negative symmetrical ones. It should be noted that since these points were assigned as material properties of the diagonal element, they needed to be transformed into equivalent stresses ($\sigma = P / (A \times \cos\theta)$) and strains ($\varepsilon = \Delta \times \cos\theta / L$). In the above equations (P) is the lateral force, (A) the area of one pair of straps, (Δ) the lateral displacement, (L) the initial diagonal length and (θ) the angle of the diagonal (see Fig. 5).

The pinching controlling parameters (rDispP, rForceP, uForceP, rDispN, rForceN, and uForceN) were obtained through a calibration process. Their values were iteratively modified, aiming to reach the best agreement between the OpenSees analysis and the actual cyclic response from ABAQUS models and to minimise the difference in the cumulative dissipated energies. The results indicated that, in general, these parameters are not very sensitive to the

imposed vertical load level. Following the calibration process, the pinching parameter values of (rDispP=0.9, rForceP=0.03, uForceP=0, rDispN=0.9, rForceN=0.03, and uForceN=0) were found to be suitable for all cases, and therefore, these values were used in the analyses henceforth.

The accuracy of the equivalent OpenSees model was investigated for two cased study examples. Wall SW1 had no additional vertical load and failed because the straps reached their ultimate strain. Wall SW2 had an additional vertical load equal to 29% of its axial load capacity (P_w), and its failure mode was the premature buckling of the compressive chord stud before the straps reached their ultimate strain. Fig. 7 compares the monotonic lateral load-displacement responses of these wall specimens.

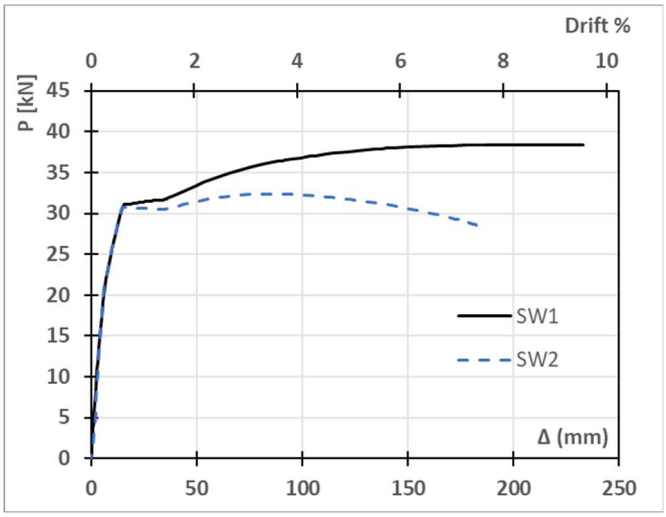

Fig. 7 Lateral load-displacement relationships for walls SW1 and SW2

In Fig. 8, the accuracy of the "Pinching4" model is verified by comparing the hysteretic response of the SW1 and SW2 models in ABAQUS and OpenSees, in terms of lateral-load displacement curves and the cumulative dissipated energy. It can be observed from Fig. 8a and Fig. 8b that for both cases, there was a good agreement between the hysteretic lateral load-displacement curves with respect to the initial stiffness and the maximum capacity (P_u). Regarding the cumulative dissipated energy, the average error was 8.6% for wall SW1 and 4.5% for wall SW2 (see Fig. 8c and Fig. 8d).

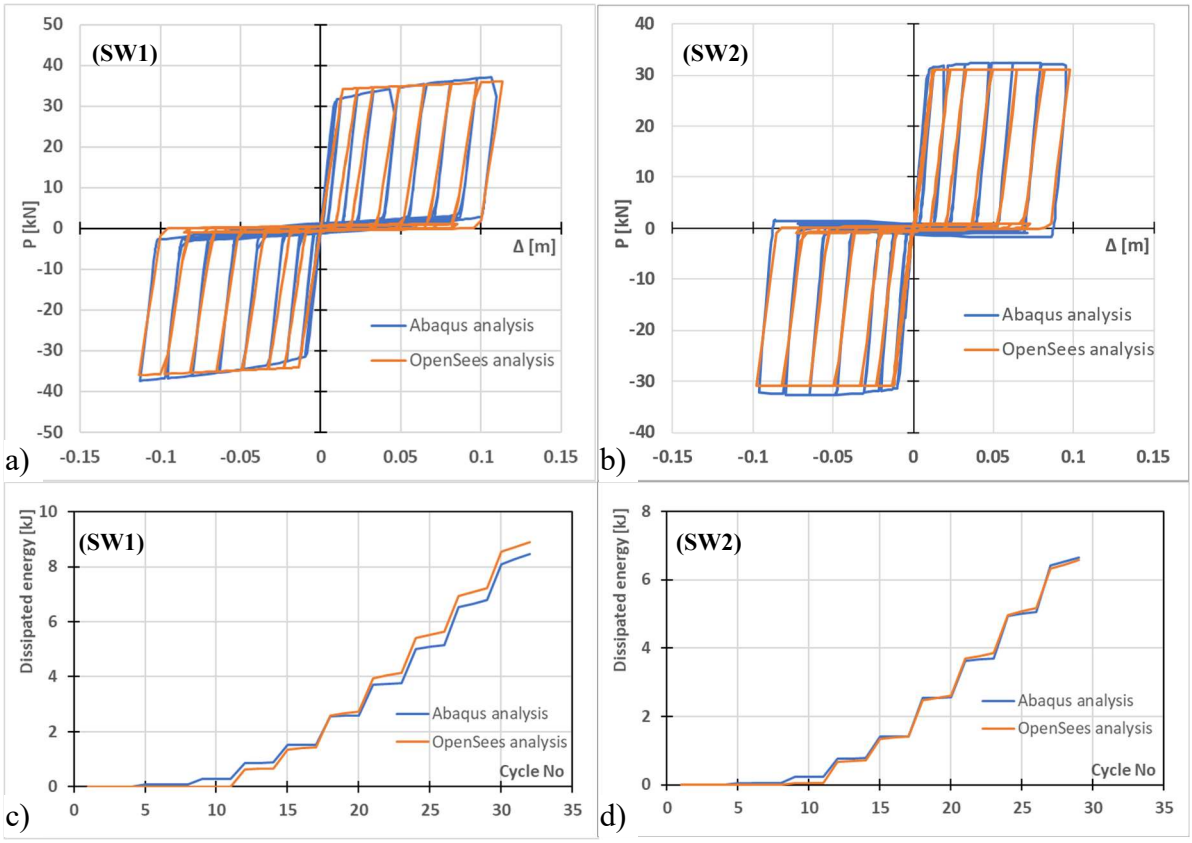

Fig. 8 ABAQUS and OpenSees hysteretic response and cumulative energy of (a & c): SW1 wall and (b & d): SW2 wall

3.4 Multi-storey frame system

The previously verified non-linear OpenSees models of the single strap-braced wall panels were employed to develop the multi-storey frame models, as depicted in Fig. 9. The chord studs and the intermediate studs were modelled as elastic truss elements, not transferring any moments. Assuming that the flooring system provided a rigid diaphragm action, the top and bottom tracks were modelled as elastic beam-column elements of very high stiffness, connected at their endpoints with "bar"-type rigid links. At each storey level, the hysteretic behaviour for the walls was characterised by "Pinching4" material properties assigned to each diagonal element through the backbone curve parameters obtained from the corresponding ABAQUS monotonic results (see Section 3.3). In order to account for second-order effects, a P-Δ frame was attached to the main CFS frame [23,45]. It comprised a leaning column on each level [46],

399 modelled as an elastic beam-column element with a high axial and low flexural stiffness. The
400 leaning columns were connected to the main frame through rigid beams, modelled by rigid
401 truss elements, using zero-length hinge elements at both ends (see Fig. 9). The horizontal
402 movement of the leaning column end nodes was constrained relative to their adjacent nodes of
403 the main frame at each level.

404 The vertical loads and the storey masses, calculated in Section 2.2, were applied as
405 uniformly distributed on the track elements at the top of each floor level, while a concentrated
406 vertical force equal to the total gravity load of each storey was applied at the joints of the P-Δ
407 frame. Following gravity analysis, a modal analysis was performed. For the dynamic analyses,
408 a Rayleigh damping value of 2% was considered as suggested by [23,45].

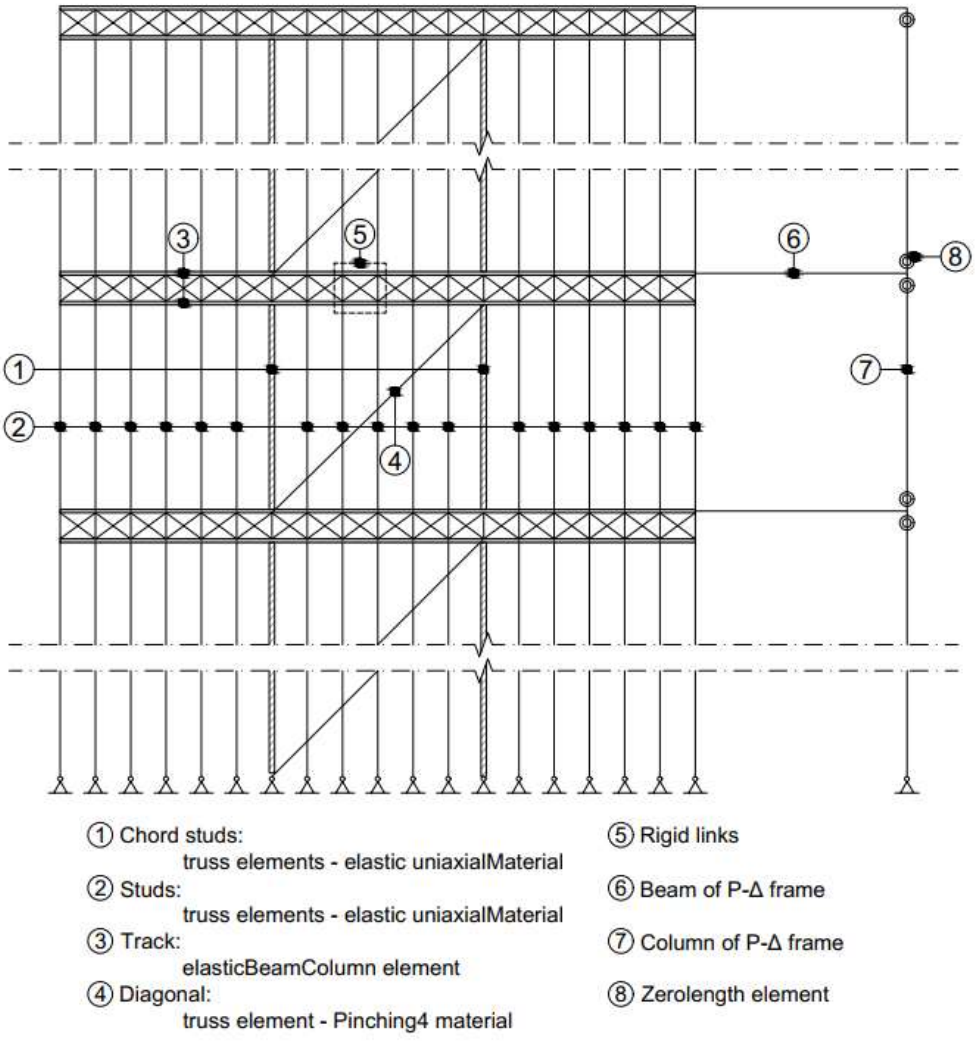

409
410 **Fig. 9** The strap-braced wall frame model in OpenSees

4 Non-linear time-history analysis

To evaluate the performance of CFS strap-braced wall frame systems and assess the efficiency of the proposed design methodology under seismic excitations, the Eurocode and the proposed design solutions were subjected to non-linear time-history analyses by selecting appropriate artificial and real ground motion records. The ductility demand and capacity of the systems were compared, and their expected overall structural damage, expressed by a global damage index, was calculated.

4.1 Artificial spectrum-compatible ground motion records

The elastic response spectrum per Eurocode 8 [29] was produced for a ground acceleration value of 0.35 g, soil category B, and importance class II. This response spectrum was used for the seismic design of the frames, as discussed in Section 2.2. Seven compatible artificial records (Syn1-Syn7) were then generated with SeismoArtif software [47] to match the design spectrum. In this study, artificial records were initially utilised to assess the seismic performance of the design solutions as representatives of the selected design spectrum [48–50]. Fig. 10 demonstrates the good agreement between the response spectra of the artificial records and the Eurocode 8 design response spectrum.

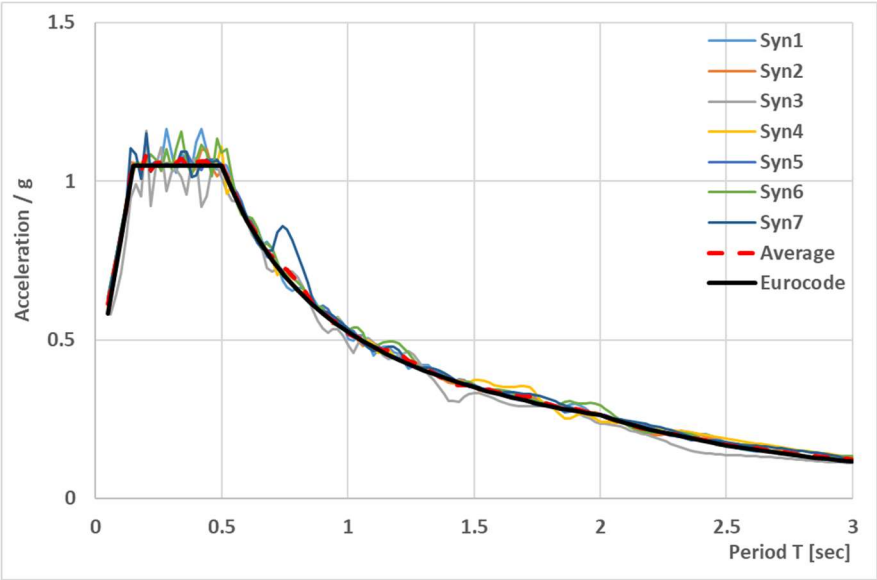

Fig. 10 Comparison between elastic response spectra of artificial records and the selected Eurocode 8 design spectrum

4.2 Performance Assessment Parameters

For performance-based design and assessment of structures, ASCE/SEI 41-17 [51] specifies three seismic performance objectives: Immediate Occupancy (IO), Life Safety (LS) and Collapse Prevention (CP). Each performance objective is represented based on acceptance criteria corresponding to a specific ground motion intensity level. In this study, the Design-Basis Earthquake (DBE), corresponding to (LS) performance target, had a PGA = 0.35 g consistent with the adopted design response spectrum. The Maximum Considered Earthquake (MCE), associated with (CP) level, had a PGA= 0.5 g (1.5 times the DBE level as recommended by ASCE 7-05 [52]). The PGA of the Frequent Earthquake (FE), corresponding to (IO) performance level, was set to 0.1 g. It should be noted that for practical applications, these earthquake intensity values should be obtained based on the results of the seismic hazard assessment of the selected site.

In general, the seismic performance of structures is measured based on Engineering Demand Parameters (EDP), such as inter-storey drift, roof displacement, plastic hinge rotation,

445 and peak storey ductility [53,54]. ASCE/SEI 41-17 [51] prescribes limits for the storey ductility
446 demand ($\mu_i = \Delta_{inelastic,i} / \Delta_{y,i}$) corresponding to (IO), (LS) and (CP) performance levels.
447 ($\Delta_{inelastic,i}$) and ($\Delta_{y,i}$) stand for the drift demand and wall drift at yield at storey (i). In this study,
448 ($\Delta_{y,i}$) was calculated based on the idealised bilinear load-displacement curves, as prescribed in
449 ASCE/SEI 41-17 [51] , using the results of ABAQUS models. The ductility limits for wall
450 systems employing dogbone-shaped diagonal straps were set at 3.2, 7.3 and 10.1, for
451 performance levels (IO), (LS) and (CP), respectively [51].

452 The ductility capacity of the walls at each storey level were calculated in accordance with
453 the dominant failure mode (i.e. failure of the straps reaching their ultimate strain, or buckling
454 of the compressive chord stud). To calculate the ductility capacity ($\mu_{c,i} = \Delta_{u,i} / \Delta_{y,i}$), the ultimate
455 wall drift ($\Delta_{u,i}$) was considered as the drift corresponding either to the respective failure mode
456 or a 20% drop in the maximum lateral load, whichever occurs first.

457 The efficiency and reliability of the design solutions were also assessed based on the
458 cumulative global damage model proposed by Krawinkler [55] and Powell and Allahabadi [56],
459 measuring the change in the dissipated energy relative to the displacement demands. In this
460 work, the damage index (DI_i) of each storey (i) was selected to be a function of the inter-storey
461 drift demands [48,49]:

$$DI_i = \sum_{j=1}^{N} \left(\frac{\Delta\delta_{pj}}{\Delta \mathrm{y,i}} \right)^c \tag{5}$$

462 where ($\Delta\delta_{pj}$) is the inelastic inter-storey drift at the j-th excursion, (N) the total number of the
463 inelastic excursions, ($\Delta_{y,i}$) the inter-storey drift at yield, and (c) is a constant parameter
464 accounting for the stability of the hysteretic behaviour taken equal 1.5 [48].

465 To quantify the overall damage at the frame-level, the global damage index (DI_g) [48,49]
466 was used as a weighted average of the damage indices (DI_i) at each storey:

$$DI_g = \frac{\sum_{i=1}^{n} DI_i \cdot W_{pi}}{\sum_{i=1}^{n} W_{pi}} \quad (6)$$

where (DI_i) is the damage index of each storey (i), (W_{pi}) is the dissipated energy of each storey (i), and (n) is the number of storeys. The global damage index estimates the overall condition of the structure after an earthquake event and takes values between 0 (no damage) and 1 (complete damage or failure).

5 Performance evaluation of CFS strap-braced wall multi-storey frames

5.1 Seismic Performance Assessment

The seismic performance of the design solutions was assessed in terms of the maximum inter-storey drifts and storey ductility demands by scaling the seven artificial records (Syn1 to Syn7) to 0.1 g, 0.35 g and 0.5 g, corresponding to (IO), (LS) and (CP) performance levels (see Section 4.2). As per Eurocode 8 [29], since the results of at least seven time-history analyses are obtained, their average response can be used for design purposes. Therefore, for each of the three performance levels, the inter-storey drift distributions for both design solutions were obtained under the seven spectrum compatible artificial records. Fig. 11 illustrates the average and average plus standard deviation of the results. In general, the results indicate that the inter-storey drift distributions were more uniform in the proposed design solution compared to its code-compliant counterpart, especially under higher earthquake intensity levels. The proposed design method could also reduce the maximum inter-storey drifts, on average, by around 10% and 20% under (LS) and (CP) earthquake intensity levels, respectively.

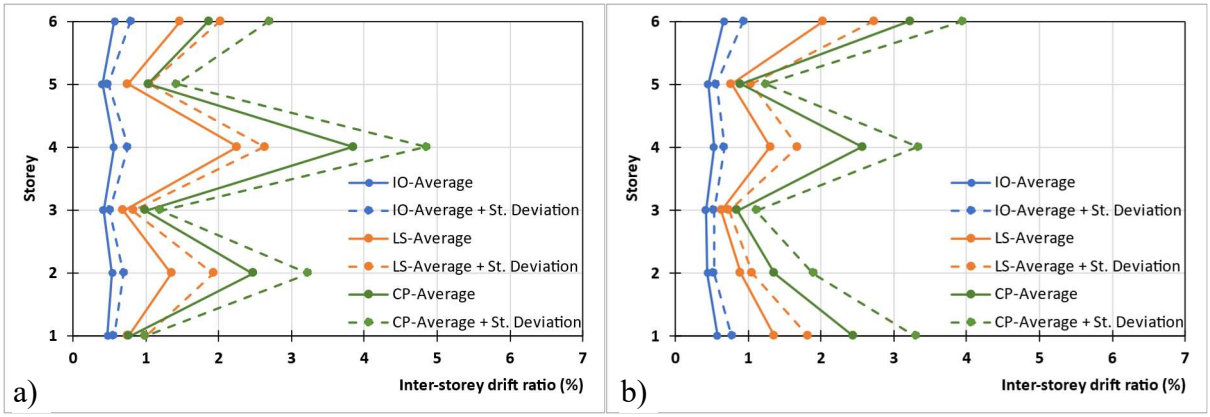

Fig. 11 Inter-storey drift distribution of a) Eurocode design and b) Proposed design under seven artificial spectrum compatible records

Fig. 12 to Fig. 14 display the average and the average plus standard deviation distribution of the storey ductility demands of the Eurocode and the proposed design solutions for (IO), (LS) and (CP) performance levels, respectively. The code ductility limits and the ductility capacity of each storey are also plotted for comparison purposes (see Section 4.2). It is shown in Fig. 12 that both frames could satisfy the code ductility limit of 3.2 for the (IO) performance level. The storey ductility capacity values (obtained from ABAQUS models) were also above the demand values for both cases. However, the proposed design solution provided a considerably higher safety margin in this case. The results presented in Fig. 13 indicate that, on average, both frames satisfied the code ductility limit of 7.3 for the (LS) performance level. However, the average plus standard deviation ductility marginally exceeded this limit at the 4th storey of the Eurocode design solution. Moreover, it is shown that the average storey ductility demands at the 2nd and 4th storey of the Eurocode design were considerably higher than their corresponding capacity values. This indicates that the Eurocode frame exhibited a soft-storey mode of failure at these storey levels due to the premature buckling of the compressive chord studs, not allowing the diagonal straps to reach their ultimate capacity. This confirms that satisfying the code suggested ductility demands by ignoring the effects of vertical loads may lead to unsafe design solutions. It can be seen that this issue was addressed by using the proposed design method, as the storey ductility capacities were always considerably higher

508 than the demand values. For the (CP) performance level, Fig. 14 shows that the code ductility
509 limit of 10.1 was exceeded, by 13% at the 4th storey of the code design solution, while it was
510 fully satisfied in the proposed design solution. The storey ductility demands at the 2nd, 3rd, 4th
511 and 5th storey levels of the Eurocode design frame were also exceeded their capacity values,
512 indicating a premature failure mechanism under this earthquake intensity level. Similar to the
513 previous case, by adopting the proposed design method, the capacity values were always
514 considerably above the storey ductility demands at all storey levels.
515

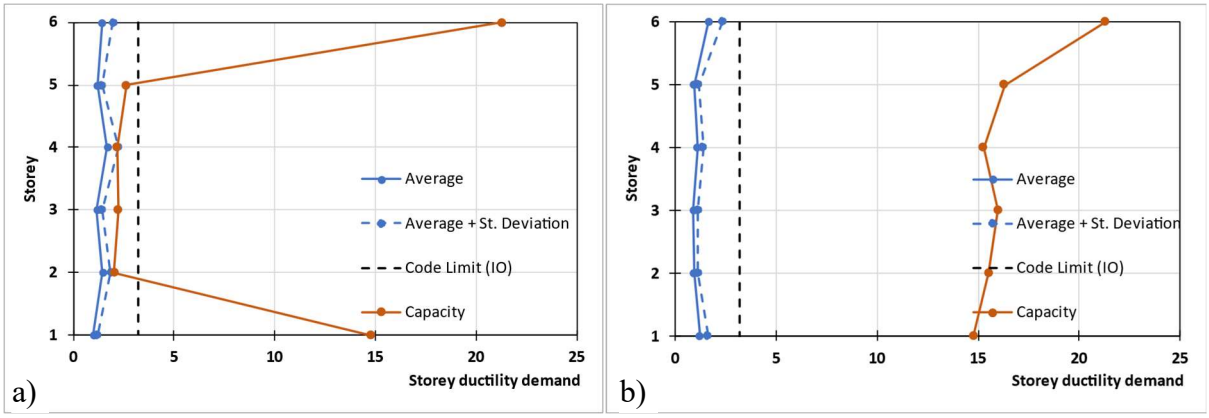

516

517 **Fig. 12** Storey ductility demand and capacity distribution of a) Eurocode design and b) proposed
518 design under seven artificial spectrum compatible records, IO performance limit
519
520

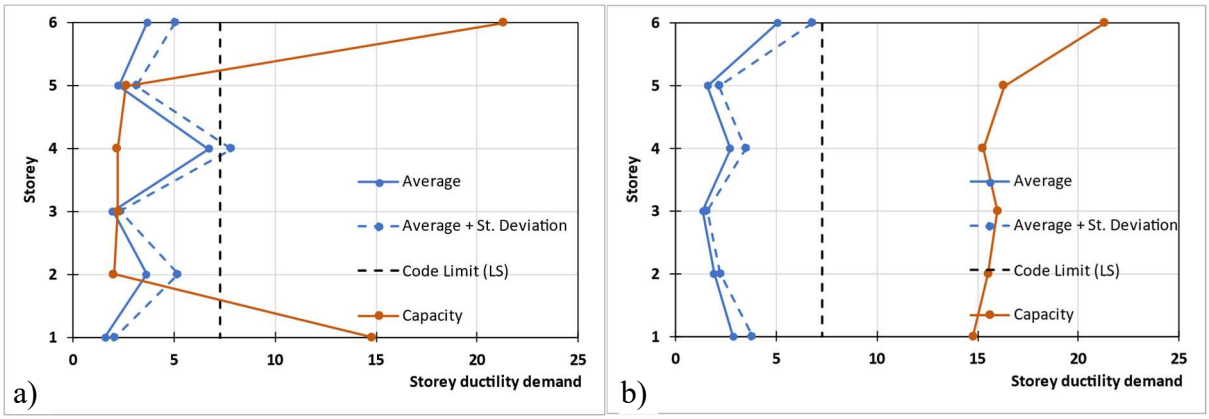

521

522 **Fig. 13** Storey ductility demand and capacity distribution of a) Eurocode design and b) proposed
523 design under seven artificial spectrum compatible records, LS performance limit
524

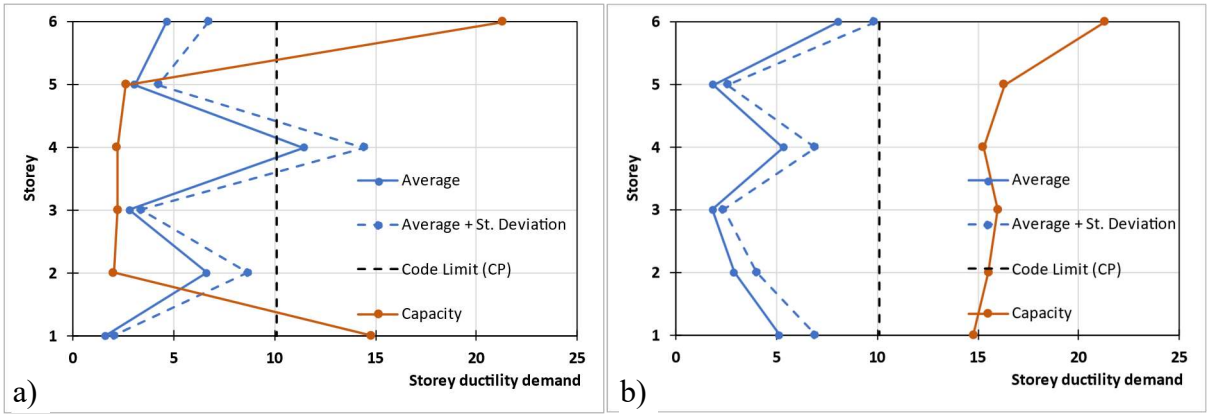

Fig. 14 Storey ductility demand and capacity distribution of a) Eurocode design and b) proposed design under seven artificial spectrum compatible records, CP performance limit

5.2 Non-linear Incremental Dynamic Analysis (IDA)

Incremental Dynamic Analysis (IDA) is a numerical method to assess the performance and vulnerability of structures under seismic loads [54,57]. The studied structure is subjected to ground motion records scaled to a progressively increased intensity, and its structural performance is evaluated using a response parameter such as maximum roof displacement or global damage index. In this study, IDA was performed on the Eurocode and the proposed design solutions subjected to the seven artificial spectrum-compatible ground motion records, as was described in Section 4.1. The PGA of the input earthquakes was considered as the intensity parameter to be consistent with the limits used for the ASCE/SEI 41-17 [51] performance targets (see Section 4.2).

The average and average plus standard deviation of the global damage index (DI_g) values for the Eurocode and the proposed design solutions subjected to the artificial spectrum-compatible records at different intensity levels are shown in Fig. 15. Due to the low ductility capacity of some storey levels, the Eurocode design frame exhibited a high level of damage even under low intensity records. It is shown that the global damage index for the Eurocode design solution was around 40% at PGA= 0.10 g (IO performance level), while the frame was completely damaged under the PGA levels above 0.20 g. This clearly indicates that the frame

did not comply with the performance targets of the seismic design codes. As discussed before, this is mainly attributed to the buckling of the compressive studs due to the negligence of the P-Δ secondary moment effects during the code-base design process.

The improved proposed design frame, on the other hand, experienced considerably lower damage compared to its code-compliant counterpart at all earthquake intensity levels. By adopting the proposed design method, the frame exhibited a global damage index of 4%, 26% and 58% at PGA levels of 0.10 g (IO performance level), 0.35 g (LS performance level) and 0.5 g (CP performance level), respectively. The full damage (DI_g=100%) in this case was reached only at PGA levels above 0.65 g. In general, these results confirm that the proposed design solution fulfils the expected performance targets for typical building structures.

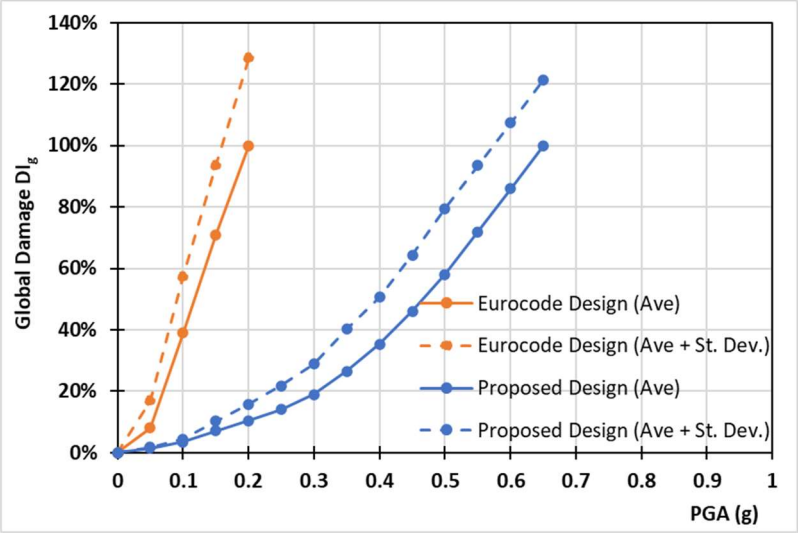

Fig. 15 Global damage index (DI_g) for the Eurocode and proposed design solution frames subjected to artificial spectrum-compatible ground motion records

5.3 Seismic performance under real ground motion records

In this section, the seismic performance of the Eurocode and the proposed design solutions are assessed under compatible real ground motion records. A set of twenty earthquakes from the Pacific Earthquake Engineering Research Centre (PEER) ground motion database [58]

were selected to be compatible with the selected elastic design response spectrum of Eurocode 8 [29]. All the accelerograms were obtained for a combination of near and far-field earthquakes with magnitudes between 6.8 and 7.6 (i.e. medium to strong earthquake records). The characteristics of the selected records are summarised in Table 5, and their respective response spectra are compared with the Eurocode design spectrum in Fig. 16. In Table 5, (R_{rup}) is the site distance from the epicentre, and (V_{s30}) is the average shear wave velocity, with the search range set between 360-800 m/sec, to match ground type B, per Eurocode 8 [29]. It is shown in Fig. 16 that the average of the earthquake response spectra of the selected records compares very well with the Eurocode design spectrum used in the design process of the frames (see Section 2.1). Therefore, these records were used without scaling.

Table 5 Real ground motion records

Record name	Earthquake Name	Year	Magnitude	R_{rup} (km)	V_{s30} (m/sec)
E1	"Loma Prieta"	1989	6.93	10.72	476.54
E2	"Loma Prieta"	1989	6.93	3.85	462.24
E3	"Loma Prieta"	1989	6.93	8.5	380.89
E4	"Cape Mendocino"	1992	7.01	8.18	422.17
E5	"Kobe_ Japan"	1995	6.9	7.08	609
E6	"Chi-Chi_ Taiwan"	1999	7.62	5.8	624.85
E7	"Chi-Chi_ Taiwan"	1999	7.62	7.08	468.14
E8	"Chi-Chi_ Taiwan"	1999	7.62	2.74	614.98
E9	"Chi-Chi_ Taiwan"	1999	7.62	8.2	443.04
E10	"Chi-Chi_ Taiwan"	1999	7.62	10.97	363.99
E11	"Chi-Chi_ Taiwan"	1999	7.62	9	671.52
E12	"Chi-Chi_ Taiwan"	1999	7.62	45.18	446.63
E13	"Manjil_ Iran"	1990	7.37	12.55	723.95
E14	"Cape Mendocino"	1992	7.01	18.31	459.04
E15	"Cape Mendocino"	1992	7.01	19.32	387.95
E16	"Chuetsu-oki_ Japan"	2007	6.8	11.94	383.43
E17	"Chuetsu-oki_ Japan"	2007	6.8	16.86	561.59
E18	"Chuetsu-oki_ Japan"	2007	6.8	20.03	561.59
E19	"Chuetsu-oki_ Japan"	2007	6.8	20	561.59
E20	"Iwate_ Japan"	2008	6.9	12.85	512.26

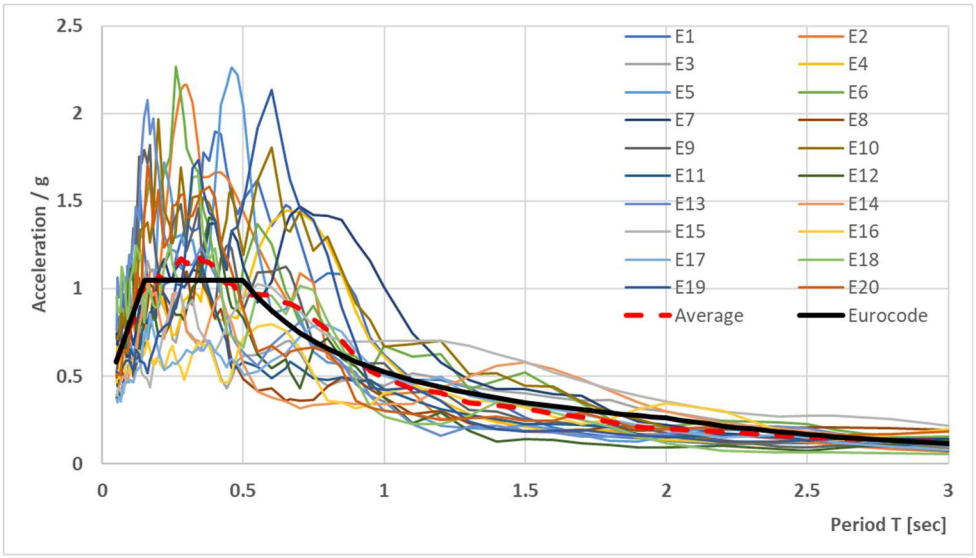

Fig. 16 Comparison between the response spectra of the real earthquakes and the elastic design response spectrum of Eurocode

The Eurocode and the proposed design frames were subjected to the set of the real earthquake records, and the average and the average plus standard deviation of inter-storey drift distributions were calculated as displayed in Fig. 17. It can be noted that the average inter-storey drift patterns were almost similar to those under artificial spectrum-compatible ground motions, which confirms the general agreement between the artificial and real records. The Eurocode design frame reached a maximum average inter-storey drift value of 2.4% (average plus standard variation of 3.6 %), while the maximum average inter-storey drift value slightly increased to 2.7% (average plus standard variation of 3.6 %) in the proposed design solution.

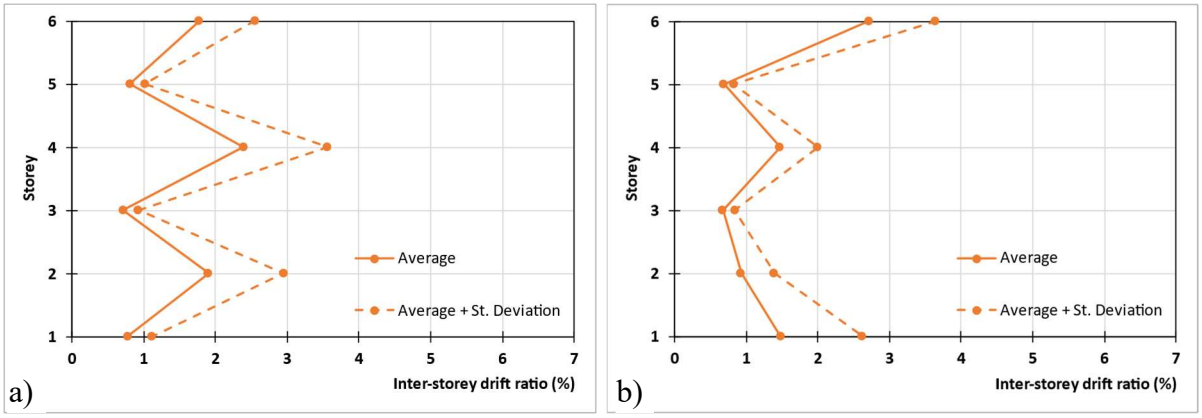

Fig. 17 Inter-storey average drift distribution for (LS) performance limit of a) the Eurocode design and b) the proposed design solutions subjected to real ground motion records

The average and the average plus standard deviation of storey ductility demands for the Eurocode and the proposed design solutions are shown in Fig. 18. The average storey ductility demands for the Eurocode design frame were always below the code limit of 7.3 for the (LS) performance level. However, at the 2nd and 4th storey levels, they exceeded the ductility capacity by 2.5 and 3.2 times, reaching values of 5.1 and 7.2, respectively. As discussed before, this can lead to extensive damage in the Eurocode design structure under strong earthquake events.

The average storey ductility demand for the proposed design solution reached a maximum value of 6.8, which means the frame satisfied the code (LS) performance level. Besides, the results indicate that in the proposed design frame, the average storey ductility demands were always well below the storey ductility capacity values. It is shown that the adopted design methodology could significantly increase the ductility capacity of the storeys that initially suffered from the premature failure of the compressive chord studs. These results are consistent with those observed under artificial records in Section 5.1.

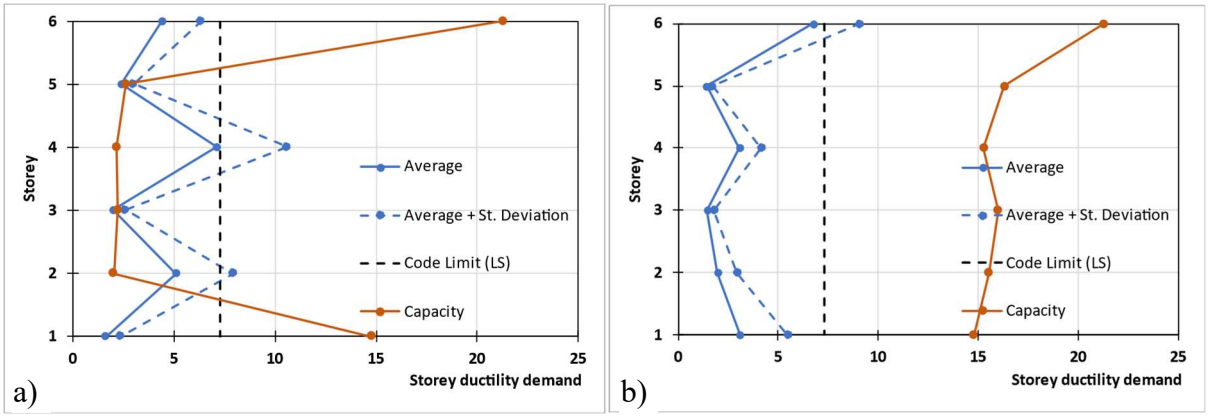

Fig. 18 Average storey ductility demand and capacity for (LS) performance limit of a) the Eurocode design and b) the proposed design solutions subjected to real ground motion records

The global damage indices (DI_g) for the Eurocode and the proposed design solutions were also calculated under the set of 20 real ground motion records (E1 to E20), as plotted in Fig. 19. For the Eurocode design frame, the global damage index was very high for all the selected

616 records, indicating an unacceptable level of damage leading to complete collapse in most cases.
617 The global damage index for the proposed design solution ranged between 10% and 63%, with
618 an average value of 40%. This significant improvement in the seismic performance of the
619 modified frame is attributed to the higher ductility capacity of the system achieved by taking
620 into account the effects of vertical loads on the lateral load capacity and ductility of the wall
621 panels in the design process. The results of this study, in general, highlight the efficiency of
622 the proposed method, which should prove useful in the preliminary design of multi-storey CFS
623 strap-braced frames in seismic regions.
624

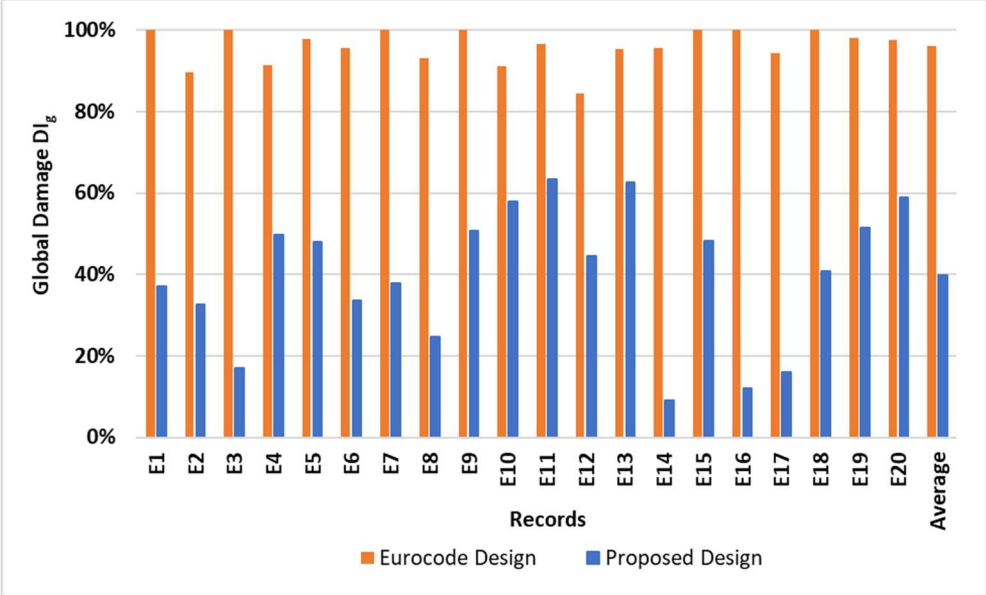

625

626 **Fig. 19** Global damage index (DI_g) for the Eurocode and proposed design solution frames subjected to
627 a set of real ground motion records
628

629 ## 6 Summary and Conclusions

630 This study aimed to investigate the efficiency of the Eurocode and a newly developed
631 methodology, which accounts for the secondary moments due to P-Δ effects, amplified by the
632 presence of additional vertical loading, for the seismic design of multi-storey CFS strap-braced
633 stud wall frames. Detailed non-linear FE models of single strap-braced wall panels were
634 developed in ABAQUS and validated against available experimental data. The validated

635 models were then adopted to develop equivalent hysteretic models in OpenSees for different
636 cross-section sizes and vertical load levels. Subsequently, a case study 6-storey CFS frame was
637 designed per Eurocode 8 and the proposed methodology. The seismic performance of the
638 frames was assessed in terms of the maximum inter-storey drifts and storey ductility demands
639 under a set of artificial spectrum-compatible records scaled to (IO), (LS) and (CP) performance
640 earthquake intensity levels. For further comparison, an incremental dynamic analysis (IDA)
641 was also conducted by using a global cumulative damage index to assess the overall
642 performance of the frames. Finally, the efficiency of the two design methods was demonstrated
643 under a set of 20 real spectrum-compatible records. The study led to the following main
644 conclusions:

645 • The Eurocode 8 design solution could satisfy the ASCE/SEI 41-17 ductility demand
646 limits for (IO) and (LS) performance levels, while the ductility limit for (CP)
647 performance level was exceeded by 13%. The proposed design methodology yielded a
648 more uniform inter-storey drift distribution compared to its Eurocode 8 counterpart,
649 especially for the higher intensity levels, and met all the ductility requirements with a
650 higher safety margin.

651 • It was shown that ignoring the effects of vertical loads may lead to unsafe design
652 solutions. The Eurocode frame was completely damaged under the PGA levels above
653 0.20 g, due to the premature buckling of the compressive chord studs leading to
654 unacceptable ductility capacities at some storeys. The proposed design experienced
655 significantly lower damage at all earthquake intensity levels and exhibited a global
656 damage index of 4%, 26% and 58% at PGA levels corresponding to IO, LS and CP
657 performance levels, respectively.

658 • Both frames could satisfy the ASCE/SEI 41-17 (LS) ductility demand limits under a set
659 of design compatible real ground motion records. While the Eurocode design frame

completely collapsed in most cases, the global damage index for the proposed design solution ranged between 10% and 63%, with an average value of 40%.

- These results highlight the efficiency of the proposed methodology for the preliminary design of multi-storey CFS strap-braced frames in seismic regions.
- However, further studies are needed to investigate the efficiency of the methodology for other strap-braced wall configurations and topologies.

Declaration of competing interest

The authors declare that they have no known competing financial interests or personal relationships that could have appeared to influence the work reported in this paper.

References

[1] K. Velchev, Inelastic Performance of Screw Connected CFS Strap Braced Walls Research Report RP08-5, 2008. https://scholarsmine.mst.edu/ccfss-aisi-spec/88.

[2] M. Zeynalian, H.R. Ronagh, A numerical study on seismic performance of strap-braced cold-formed steel shear walls, Thin-Walled Struct. 60 (2012) 229–238. https://doi.org/10.1016/j.tws.2012.05.012.

[3] O. Pourabdollah, F. Farahbod, F.R. Rofooei, The seismic performance of K-braced cold-formed steel shear panels with improved connections, J. Constr. Steel Res. 135 (2017) 56–68. https://doi.org/10.1016/j.jcsr.2017.04.008.

[4] M. Zeynalian, H.R. Ronagh, S. Hatami, Seismic characteristics of K-braced cold-formed steel shear walls, J. Constr. Steel Res. 77 (2012) 23–31. https://doi.org/10.1016/j.jcsr.2012.04.009.

[5] N. Usefi, H. Ronagh, P. Sharafi, Numerical modelling and design of hybrid cold-formed steel wall panels, Thin-Walled Struct. 157 (2020) 107084.

https://doi.org/10.1016/j.tws.2020.107084.

[6] M. Gerami, M. Lotfi, Analytical Analysis of Seismic Behavior of Cold-Formed Steel Frames with Strap Brace and Sheathings Plates, 2014 (2014).

[7] A. Mirzaei, R.H. Sangree, K. Velchev, G. Comeau, N. Balh, C.A. Rogers, B.W. Schafer, Seismic capacity-based design of narrow strap-braced cold-formed steel walls, J. Constr. Steel Res. 115 (2015) 81–91. https://doi.org/10.1016/j.jcsr.2015.08.023.

[8] G. Comeau, Inelastic Performance of Welded CFS Strap Braced Walls Research Report RP08-4, 2008. https://scholarsmine.mst.edu/ccfss-aisi-spec/87.

[9] K. Velchev, G. Comeau, N. Balh, C.A. Rogers, Evaluation of the AISI S213 seismic design procedures through testing of strap braced cold-formed steel walls, Thin-Walled Struct. 48 (2010) 846–856. https://doi.org/10.1016/j.tws.2010.01.003.

[10] S. Lu, C.A. Rogers, Influence of gypsum panels on the response of cold-formed steel framed strap-braced walls, in: CCFSS Proc. Int. Spec. Conf. Cold-Formed Steel Struct., 2018: pp. 925–939. https://scholarsmine.mst.edu/isccss/24iccfss/session12/7.

[11] H. Moghimi, H.R. Ronagh, Performance of light-gauge cold-formed steel strap-braced stud walls subjected to cyclic loading, Eng. Struct. 31 (2009) 69–83. https://doi.org/10.1016/j.engstruct.2008.07.016.

[12] M. Al-Kharat, C.A. Rogers, Inelastic performance of screw-connected cold- formed steel strap-braced walls, Can. J. Civ. Eng. 35 (2008) 11–26. https://doi.org/10.1139/L07-081.

[13] S. Kasaeian, N. Usefi, H. Ronagh, S. Dareshiry, Seismic performance of CFS strap-braced walls using capacity-based design approach, J. Constr. Steel Res. 174 (2020). https://doi.org/10.1016/j.jcsr.2020.106317.

[14] P.C. Ashwin Kumar, D.R. Sahoo, Fracture ductility of hollow circular and square steel braces under cyclic loading, Thin-Walled Struct. 130 (2018) 347–361.

https://doi.org/10.1016/j.tws.2018.06.005.

[15] P.C.A. Kumar, D.R. Sahoo, Optimum range of slenderness ratio of hollow steel square braces for special concentrically braced frames, Adv. Struct. Eng. 19 (2016) 928–944. https://doi.org/10.1177/1369433216630442.

[16] P.C.A. Kumar, D.R. Sahoo, N. Kumar, Limiting values of slenderness ratio for circular braces of concentrically braced frames, J. Constr. Steel Res. 115 (2015) 223–235. https://doi.org/10.1016/j.jcsr.2015.08.026.

[17] I. Papargyriou, I. Hajirasouliha, J. Becque, K. Pilakoutas, Performance-based assessment of CFS strap-braced stud walls under seismic loading, J. Constr. Steel Res. 183 (2021) 106731. https://doi.org/10.1016/j.jcsr.2021.106731.

[18] T.W. Kim, J. Wilcoski, D.A. Foutch, M.S. Lee, Shaketable tests of a cold-formed steel shear panel, Eng. Struct. 28 (2006) 1462–1470. https://doi.org/10.1016/j.engstruct.2006.01.014.

[19] L. Fiorino, B. Bucciero, R. Landolfo, Shake table tests of three storey cold-formed steel structures with strap-braced walls, Bull. Earthq. Eng. 17 (2019) 4217–4245. https://doi.org/10.1007/s10518-019-00642-z.

[20] M.S. Lee, D.A. Foutch, Performance evaluation of cold-formed steel braced frames designed under current U.S. seismic design code, Int. J. Steel Struct. 10 (2010) 305–316. https://doi.org/10.1007/BF03215839.

[21] FEMA, FEMA 355F - State of the Art Report on Performance Prediction and Evaluation of Steel Moment-Frame Buildings, Fema-355F. 1 (2000) 1–367.

[22] G. Comeau, K. Velchev, C.A. Rogers, Development of seismic force modification factors for cold-formed steel strap braced walls, Can. J. Civ. Eng. 37 (2010) 236–249. https://doi.org/10.1139/L09-153.

[23] L. Fiorino, S. Shakeel, V. Macillo, R. Landolfo, Behaviour factor (q) evaluation the CFS

735 braced structures according to FEMA P695, J. Constr. Steel Res. 138 (2017) 324–339.
736 https://doi.org/10.1016/j.jcsr.2017.07.014.
737 [24] ATC, Quantification of building seismic performance factors, 2009.
738 [25] M.R. Davani, S. Hatami, A. Zare, Performance-based evaluation of strap-braced cold-
739 formed steel frames using incremental dynamic analysis, Steel Compos. Struct. 21 (2016)
740 1369–1388. https://doi.org/http://dx.doi.org/10.12989/scs.2016.21.6.1369.
741 [26] J. Lange, B. Naujoks, Behaviour of cold-formed steel shear walls under horizontal and
742 vertical loads, Thin-Walled Struct. 44 (2007) 1214–1222.
743 https://doi.org/10.1016/j.tws.2007.01.007.
744 [27] M. Accorti, N. Baldassino, R. Zandonini, F. Scavazza, C.A. Rogers, Response of CFS
745 Sheathed Shear Walls, Structures. 7 (2016) 100–112.
746 https://doi.org/10.1016/j.istruc.2016.06.009.
747 [28] J. Ye, R. Feng, W. Chen, W. Liu, Behavior of cold-formed steel wall stud with sheathing
748 subjected to compression, J. Constr. Steel Res. 116 (2016) 79–91.
749 https://doi.org/10.1016/j.jcsr.2015.08.028.
750 [29] CEN, Eurocode 8 : Design of structures for earthquake resistance - Part 1: General rules,
751 seismic actions and rules for buildings, European Committee for Standardization, 2004.
752 [30] AISI, AISI S400-20 North American Standard for Seismic Design of Cold-Formed Steel
753 Structural Systems, (2020).
754 [31] I. Papargyriou, I. Hajirasouliha, More efficient design of CFS strap-braced frames under
755 vertical and seismic loading, J. Constr. Steel Res. 185 (2021) 106886.
756 https://doi.org/10.1016/j.jcsr.2021.106886.
757 [32] Dassault Systèmes Simulia, Abaqus 6.14 CAE User Guide, 2014.
758 [33] S. Mazzoni, F. McKenna, M.H. Scott, G.L. Fenves, OpenSees command language
759 manual, Pacific Earthq. Eng. Res. Cent. (2007) 451.

760 http://opensees.berkeley.edu/OpenSees/manuals/usermanual/OpenSeesCommandLang
761 uageManual.pdf.
762 [34] CEN, Eurocode 3: Design of steel structures - Part 1-1: General rules and rules for
763 buildings, European Committee for Standardization, 2010.
764 [35] CEN, Eurocode 3 : Design of steel structures - Part 1-3: General rules - Supplementary
765 rules for cold-formed members and sheeting, European Committee for Standardization,
766 2003.
767 [36] CEN, Eurocode-Basis of structural design, 2002.
768 [37] N. Usefi, P. Sharafi, H. Ronagh, Numerical models for lateral behaviour analysis of
769 cold-formed steel framed walls: State of the art, evaluation and challenges, Thin-Walled
770 Struct. 138 (2019) 252–285. https://doi.org/10.1016/j.tws.2019.02.019.
771 [38] J. Ye, S.M. Mojtabaei, I. Hajirasouliha, P. Shepherd, K. Pilakoutas, Strength and
772 deflection behaviour of cold-formed steel back-to-back channels, Eng. Struct. 177 (2018)
773 641–654. https://doi.org/10.1016/j.engstruct.2018.09.064.
774 [39] J. Ye, I. Hajirasouliha, J. Becque, A. Eslami, Optimum design of cold-formed steel
775 beams using Particle Swarm Optimisation method, J. Constr. Steel Res. 122 (2016) 80–
776 93. https://doi.org/10.1016/j.jcsr.2016.02.014.
777 [40] S.M. Mojtabaei, M.Z. Kabir, I. Hajirasouliha, M. Kargar, Analytical and experimental
778 study on the seismic performance of cold-formed steel frames, J. Constr. Steel Res. 143
779 (2018) 18–31. https://doi.org/https://doi.org/10.1016/j.jcsr.2017.12.013.
780 [41] S.M. Mojtabaei, J. Becque, I. Hajirasouliha, Local Buckling in Cold-Formed Steel
781 Moment-Resisting Bolted Connections: Behavior, Capacity, and Design, J. Struct. Eng.
782 146 (2020) 04020167. https://doi.org/10.1061/(asce)st.1943-541x.0002730.
783 [42] H.S. Pham, C.D. Moen, Stiffness and strength of single shear cold-formed steel screw-
784 fastened connections, Report No. CE/VPI-ST-15-07, VirginiaTech, 2015.

785 [43] ASTM, ASTM E2126-19. Standard Test Methods for Cyclic (Reversed) Load Test for
786 Shear Resistance of Vertical Elements of the Lateral Force Resisting Systems for
787 Buildings, ASTM Int. (2019). www.astm.org.
788 [44] FEMA 356, Prestandard and Commentary for the Seismic Rehabilitation of Building,
789 Washington, D.C., 2000.
790 [45] I. Shamim, C.A. Rogers, Numerical evaluation: AISI S400 steel-sheathed CFS framed
791 shear wall seismic design method, Thin-Walled Struct. 95 (2015) 48–59.
792 https://doi.org/10.1016/j.tws.2015.06.011.
793 [46] L.F. Geschwindner, A practical look at frame analysis, stability and leaning columns,
794 Eng. J. 39 (2002) 167–181.
795 [47] Seismosoft, SeismoArtif - A computer program for generation of artificial
796 accelerograms, (2018). http://www.seismosoft.com.
797 [48] N. Nabid, I. Hajirasouliha, D. Escolano Margarit, M. Petkovski, Optimum energy based
798 seismic design of friction dampers in RC structures, Structures. 27 (2020) 2550–2562.
799 https://doi.org/10.1016/j.istruc.2020.08.052.
800 [49] I. Hajirasouliha, K. Pilakoutas, General seismic load distribution for optimum
801 performance-based design of shear-buildings, J. Earthq. Eng. 16 (2012) 443–462.
802 https://doi.org/10.1080/13632469.2012.654897.
803 [50] H. Moghaddam, I. Hajirasouliha, S.M. Hosseini Gelekolai, Performance-based seismic
804 design of moment resisting steel frames: Adaptive optimisation framework and optimum
805 design load pattern, Structures. 33 (2021) 1690–1704.
806 https://doi.org/10.1016/j.istruc.2021.05.014.
807 [51] ASCE, ASCE/SEI 41-17 Seismic Evaluation and Retrofit of Existing Buildings, 2017.
808 https://doi.org/https://doi.org/10.1061/9780784414859.
809 [52] ASCE, ASCE 7-05 Minimum design loads for buildings and other structures, ASCE

Stand. (2005) 608. https://doi.org/10.1061/9780784412916.

[53] D. D'Ayala, A. Meslem, D. Vamvatsikos, K. Porter, T. Rossetto, H. Crowley, V. Silva, Guidelines for Analytical Vulnerability Assessment - Low/Mid-Rise Buildings, 2015. https://doi.org/10.13117/GEM.VULN-MOD.TR2014.12.

[54] D. Vamvatsikos, A.C. Cornell, Incremental dynamic analysis, Earthq. Eng. Struct. Dyn. 31 (2002) 491–514. https://doi.org/10.1002/eqe.141.

[55] H. Krawinkler, M. Zohrei, Cumulative damage in steel structures subjected to earthquake ground motions, Comput. Struct. 16 (1983) 531–541. https://doi.org/10.1016/0045-7949(83)90193-1.

[56] G.H. Powell, R. Allahabadi, Seismic damage prediction by deterministic methods: Concepts and procedures, Earthq. Eng. Struct. Dyn. 16 (1988) 719–734. https://doi.org/https://doi.org/10.1002/eqe.4290160507.

[57] V. Mohsenian, R. Filizadeh, Z. Ozdemir, I. Hajirasouliha, Seismic performance evaluation of deficient steel moment-resisting frames retrofitted by vertical link elements, Structures. 26 (2020) 724–736. https://doi.org/10.1016/j.istruc.2020.04.043.

[58] PEER ground motion database, https://ngawest2.berkeley.edu/. Accessed Dec, 2020.